Joint Centre for Mesoscale Meteorology, Reading, UK

A Frontal Wave Database

T. D. Hewson

Internal Report No. 85

April 1998

Met Office Joint Centre for Mesoscale Meteorology Department of Meteorology
University of Reading PO Box 243 Reading RG6 6BB United Kingdom
Tel: +44 (0)118 931 8425 Fax: +44 (0)118 931 8791
www.metoffice.com

Designed and produced by the Met Office © Crown copyright 2001 01/0240 The Met Office logo is a registered trademark.

A Frontal Wave Database

Tim Hewson

This document describes the database on frontal waves being developed at JCMM, Reading University. An outline of related software development is included. A number of new diagnostic quantities are referred to; those not documented elsewhere are described in Appendices.

1. Overview

Cyclones give rise to most of the significant weather observed in middle latitudes. The seeds of these cyclones are generally frontal waves. Preliminary manual studies of the handling of frontal wave / cyclone development by UKMO numerical models suggest that systematic errors exist. Over the north Atlantic the total number of systems seems to be underpredicted, with a marked shortfall southeast of Newfoundland (Figure 1). There is also evidence of systematic underprediction of both deepening and filling of cyclones, in both LAM and global model versions (see Figures 2 and 3, and also Van Der Wal and Milton (1998)). Note that Figure 3 is based on an up to date model version. Similarly there is consensus amongst forecasters that frontal waves are not well handled by numerical models. To put these observations onto a firmer footing a frontal wave database is being developed. This has become possible only recently, with the development of a fully automated model-based method for locating frontal waves (Hewson, 1997).

Past studies in this field have used methods based on surface pressure or near-surface winds. Such methods generally fail to locate cyclones early in their life-cycle. Another feature of some past studies is that they tend to use only analysis fields (to focus on climatology). The database being developed here will use a wide range of forecast lead-times as well as analysis fields. This will allow the systematic errors in the forecast, and their temporal evolution through the forecast period, to be fully documented. The database will also contain a very wide range of diagnostic information for each frontal wave. Such information may in future enable cyclonic developments which are not explicitly represented to be subjectively or objectively anticipated.

2. General Format

In October 1997 suggestions on the format of the database were sought from scientists within the Met. Office, at Reading University and at collaborating international institutions. Considerable exchange of ideas and discussions followed. Responses provided the basis for the specification provided here.

Some respondents recommended inclusion of 2 and 3-dimensional arrays of gridded model data around each frontal wave. Others recommended the inclusion of information from imagery. After internal discussion and consideration of available resources these proposals were rejected in favour of a more straightforward approach: only interpolated single point values of model diagnostics would be stored for each frontal wave. It was noted that many of the diagnostics, such as 'vertical velocity due to Q-G forcing', implicitly take into account the atmospheric structure well beyond a point in question. Similarly, inclusion of imagery at this stage would add considerable complexity to the task; a simple 2-D tabular format for the data would enable systematic studies using imagery to be easily carried out by interested parties at a later stage.

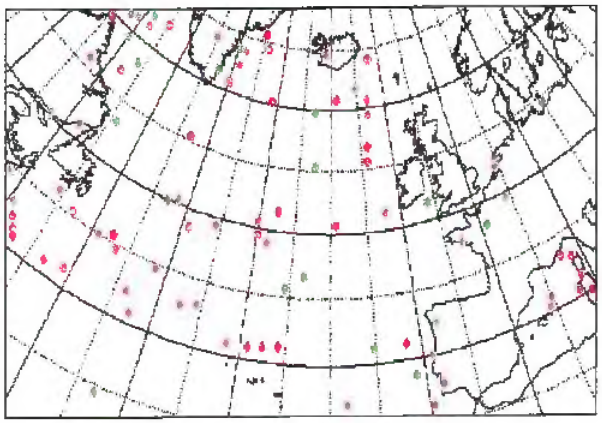

Figure 1. Verification of 00z weekday global model forecasts, for T+72, T+96 and T+120 for period 15th Jan 1996 - 15th March 1996. Red dots show positions of analysed low centres and prominent waves for which no counterpart in a particular forecast could be found. Green dots show forecast low centres and prominent waves for which no counterpart in the analysis could be found. Verification was subjective.

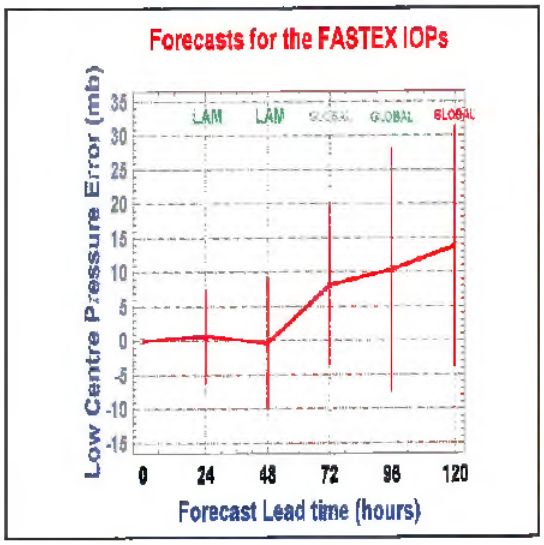

Figure 2. Verification of unified model forecasts for lows observed as IOPs during the FASTEX period - Jan and Feb 1997. Verification times centre on when the true low was within the box 10-25W, 45-60N. Average sample size is about 15. Vertical bars show one standard deviation. There is inherent bias in the sample towards lows which were 'well' forecast.

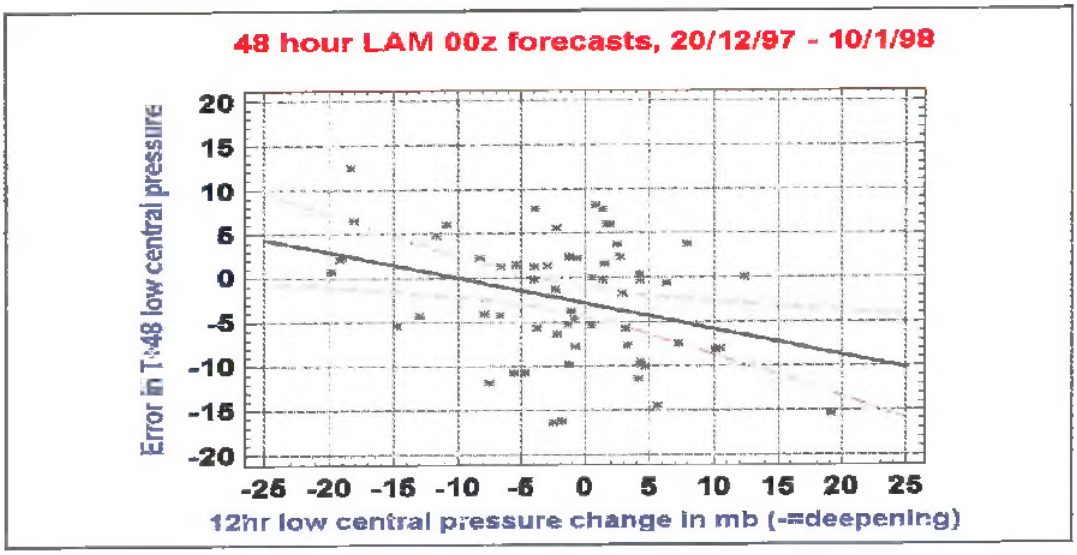

Figure 3. Verification of 48 hour LAM 00z forecasts for the box 60W-5E, 40N-65N, for the period 20/12/97 to 10/1/98. The error in low central pressure (that is pressure at centre of forecast low minus pressure at centre of analysed low) is plotted against *true* deepening/filling rate at verification time (uses 18z and 06z LAM analyses spanning the verification times). Black line is based on simple linear regression (R=−0.34), with 95% confidence limits added. This line implies some systematic under-filling of filling depressions, and (to a lesser extent) some systematic under-deepening of rapidly deepening depressions.

3. Temporal and Spatial Coverage

It is planned that there will be several stages of development of the database, during which both temporal and spatial coverage will be expanded:

(1)

Area:	North Atlantic
Real-Time?:	No
Model:	LAM
Input data resolution:	~100km interpolated
Temporal Coverage:	FASTEX period, Jan+Feb 1997
Forecast range:	T+0 to T+48, 3 hr steps.
Time Scale:	Spring 1998

(2)

Area:	North Atlantic
Real-Time?:	Yes
Model:	New UM configuration. First model run†.
Input data resolution:	~100km interpolated
Temporal Coverage:	1 Forecast per day (00z). Possibly extend to 4 per day.
Forecast range:	T+0 to T+48, 3 hr steps. Perhaps 6hr steps to T+120 for second run†.
Time Scale:	Summer 1998

(3)

Area:	Global
Real-Time?:	Yes
Model:	New UM configuration. Second model run†.
Input data resolution:	~60km
Temporal Coverage:	2 Forecasts per day (00z and 12z)
Forecast Range:	T+0 to T+144, 6hr steps.
Time Scale:	Summer 1999

Stages (1) and (2) can be achieved with existing resources. Expansion to the global domain in stage (3) will require considerable extra resources - primarily computing power, support and disk space, as outlined in section 5 below - and will thus depend critically on their availability, as well as on the preliminary results of stages (1) and (2).

[†The 'first' and 'second' model runs are the new equivalents of, respectively, the old LAM and global model runs]

4. Identification of a Frontal Wave

Hewson's (1997) definition of an objective frontal wave (tip), which consisted of a set of equations ([L?]) and inequalities ([M?]), will be used for the frontal wave database. His definition can be broken down as follows: 'Frontal wave tips are located on the warm air side of regions of low-level Theta-W gradient **[L1]** where the geostrophic Theta-W advection is zero **[L2]** *and* the

cross-front change in thermal gradient is sufficiently large **[M1]** *and* the Theta-W gradient in the adjacent baroclinic zone is sufficiently large **[M2]** *and* the relative vorticity of the cross-front wind is greater than zero **[M3]**'. Together **[L1]**, **[L2]**, **[M1]** and **[M2]** identify the meeting points of cold and warm objective fronts, whilst criterion **[M3]** removes those meeting points which are 'anti-waves' and not waves. Hewson (1997) did not include a complete description of why **[M3]** relates to the vorticity of the cross-front wind; this is given below in Appendix 1.

Several examples of objectively identified frontal waves can be seen on Figure 4 (as well as potential waves, described in section 5); note that the thick red/blue lines, ie the fronts, are really contours satisfying **[L1]** (some have end points due to the effects of **[M1]** and **[M2]**), whilst the thin blue lines are contours satisfying **[L2]**. The places where these two contour fields intersect, and where **[M3]** is also satisfied, are then the tips of objective frontal waves.

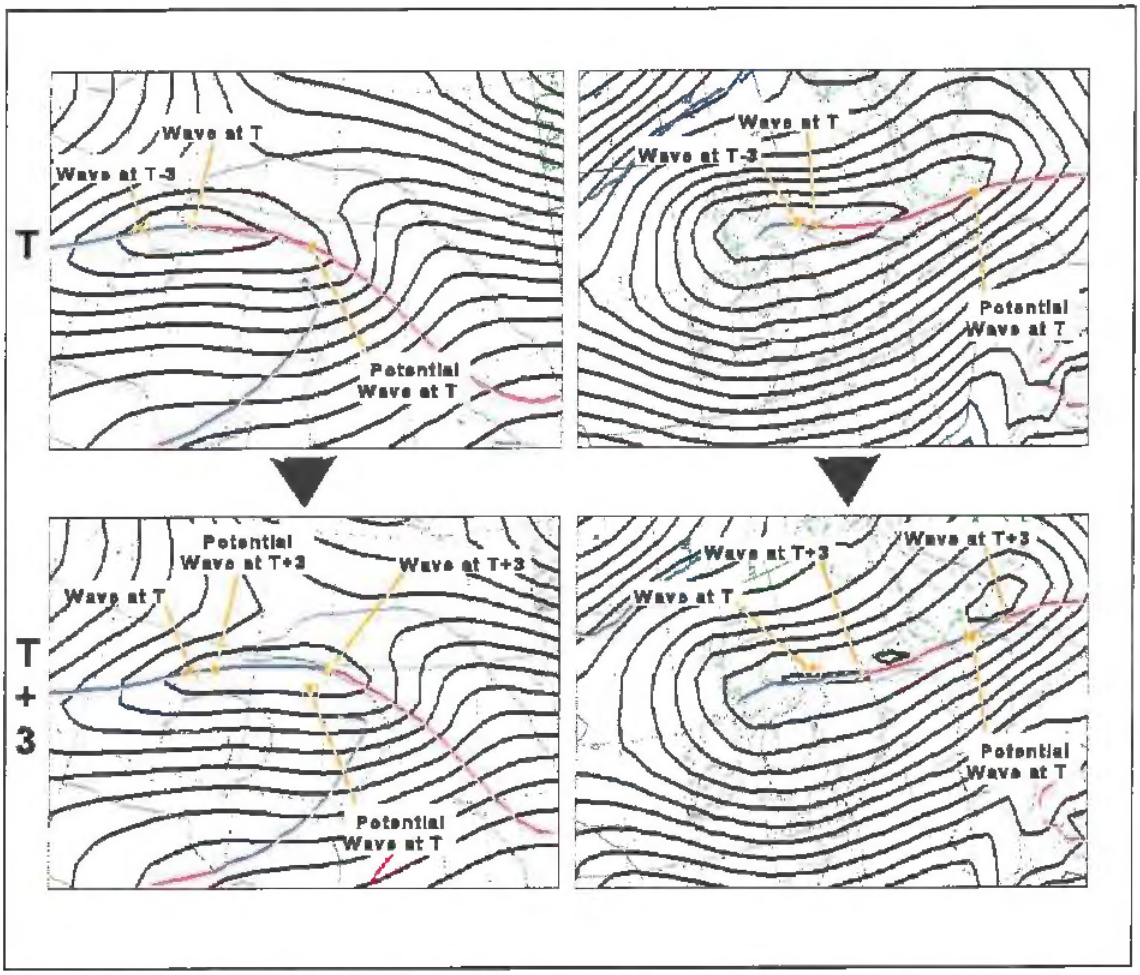

Figure 4: Two UM examples (one left, one right) showing objective frontal waves, and their evolution through a 3 hour period (upper panels are for time T, lower panels for T+3). Each example shows a potential wave at time T which becomes a true frontal wave by T+3. Thick red and blue lines are warm and cold objective surface (900mb) fronts; black contours are mean sea level pressure (2mb interval). Orange dots show tips of waves and potential waves, as labelled; bracketed dots are for 3 hours before frame time - included to demonstrate continuity. Thin blue contours denote geostrophic advection of theta-W (at 900mb) equals zero (equation **[L2]**). In both examples potential waves at time T exist close to a parent frontal wave/low; in the right example the parent wave/low maintains identity between T and T+3, in the left example it degenerates into a potential wave as the newer wave develops. T is 12z, 7 March 1998.

Hewson (1997 and 1998) recommended using data from the 900 hPa level to identify objective surface fronts and frontal waves. More recent work indicates that a marked reduction in the

generation of spurious objective frontal waves (and to a lesser extent spurious fronts) near to regions of high topography, and greater self-consistency can be obtained by using, instead, an interpolated model surface whose height is everywhere 1km above the earth's surface. This can, to an accurate approximation, be defined as the surface where:

$$\phi - Z_{orog} = 1\text{km}$$

where ϕ is geopotential height and Z_{orog} is the height of the model orography. This will be referred to as the '1km surface'.

5. 'Potential' Frontal Waves

Section 4 deals with 'actual' frontal waves. This is somewhat limiting in that there will be no record, in the database, of frontal segments which theoretical ideas (see for example Bishop and Thorpe (1994)) suggest might otherwise be well-suited to frontal wave development. One could address this problem by saving data at regularly spaced intervals along every front. However this would increase dramatically both storage space required, and program run time. An alternative would be to replace the criterion of there being zero geostrophic thermal advection **[L2]**, in the frontal wave tip definition, with the following:

'The along-front gradient of the vorticity of the cross-front geostrophic wind is zero' **[L3]**

This will pinpoint small nuances in the wind/pressure field that correspond, in both synoptic and dynamical terms, with 'potential frontal waves' (new terminology). To avoid the potential wave definition encompassing also true frontal waves (ie 'double-counting'), one additional criterion is also required. This states that:

'There is no along-front change in the sign of the cross-front wind' **[M4]**

We thus define a Potential Frontal Wave (tip) to be any point in space, on the 900mb, or preferably 1km surface, that satisfies **[L1]**, **[L3]**, **[M1]**, **[M2]**, **[M3]** and **[M4]**. This is discussed fully in Appendix 2.

Figure 4 illustrates potential frontal waves, showing how they relate to the structure seen on an (objectively-produced) surface chart; note that the potential waves are located close to weaknesses in the pressure pattern. The figure also shows potential waves evolving into real frontal waves (during the 3 hour period between upper and lower panels), as well as one example of a real frontal wave 'degenerating' into a potential wave. Further discussion and examples of both warm and cold front wave developments can be found in Kurz (1995).

6. Data Generation

One aim of this project is to automate the entry of data into the database. The work required has four key components:

(i) Generate *basic* diagnostics from model data
(ii) Identify the locations of the frontal waves
(iii) Extract *basic* model diagnostic data at the locations derived in (i) and write to database
(iiii) Generate *supplementary* diagnostics and add these to the database

A *basic* diagnostic here is a diagnostic which can be calculated without graphical tools, whereas *supplementary* diagnostics are those whose computation does require graphical tools. There are two platforms on which components (i) to (iiii) could be carried out:

(a) VAX + PC-based DISP display system
(b) HP workstation + PV-Wave graphics package

The existing facilities and the work required for each of the four components, for each of the two platforms, are outlined below:

(i) At present the *basic* diagnostic quantities can be generated at JCMM from COSMOS fields files of fundamental variables (see Panagi, 1997).

(a) The generation of these diagnostic quantities on the VAX, for a standard north Atlantic area, is already automatic; 4 LAM forecasts and one LAM analysis are processed in this way at JCMM every day. A few of the diagnostics recommended in the table below are new, but adding these to the current package is straightforward.

(b) Code exists to run on HP workstations to generate the same variables for larger domains, at full model resolution, but this is not currently automatic. More resources would be required.

(ii) Frontal wave identification is a semi-graphical procedure, as described in Hewson (1997 and 1998).

(a) The DISP system can perform this function automatically and quickly, on a stand alone PC, without interfering with or interference from other users.

(b) PV-Wave code has also been developed to perform this function automatically. However it is slow, and, by virtue of running on a network, can affect or be affected by other users. In some ways this platform is more flexible than the PC platform. However further expenditure on resources would be required to realise this flexibility.

(iii) There is currently no code to do this.

(a) PASCAL code integrated into the DISP system will be straightforward to develop.

(b) PV-Wave code should also be straightforward to develop.

(iiii) This requires the interleaving of FORTRAN diagnostics programs and graphics.

(a) Code exists for both the diagnostic computation and the graphics, but only in a semi-automated form. Some work is required to interleave the two. A blueprint describing how this interleaving will work has been produced.

(b) There is no working code for either the diagnostics or the graphics. If a version which worked on any domain were required several man months work would be necessary to even match current levels on platform (a).

In view of the extra resources required to utilise platform (b), stages (1) and (2) in section 3 will be performed using platform (a). Stage (3) in section 3 will almost certainly have to use

platform (b). There are several possible ways of reducing the necessary work; for example the *supplementary* diagnostics could be dropped. Further proposals regarding stage (3) will be devised as results from stages (1) and (2) become apparent.

7. Content of Database

1) Layout

Data will be stored in a 2-dimensional tab-delimited tabular format, where one row, terminated by carriage return - line feed, represents one objective frontal wave identified in an analysis or forecast.

There will be no file headers or column headings in standard files. File header type information, such as date, model etc. is stored within the data columns. The tab-delimited format will render the extra space required from this approach as minimal. Standard auxiliary file(s) of column headings will be made available for concatenation onto the top of data. Thus implicit column headings will be generally consistent across files; a standard layout will be devised at the outset, and association with this will be signified by the third character in the file name extension. This methodology will allow ready concatenation of multiple data files for statistical and other analysis using a simple copy command of the form "COPY *.??A WAVES.01A".

Column headings in the auxiliary file(s) will be alphanumeric, will be case-sensitive, will contain a maximum of 8 characters each and will all begin with a letter.

Numerical data will be stored as non-decimal numeric values, with 5 digit precision, with values in the range -90000 to 90000 permissible for true values. 99999 will be the missing data indicator. Suitable scalings and units for each data element are given in the table below, and will be made available as additional concatenatable auxiliary files. Chosen scalings for many quantities assume a 'typical' table entry will be of order 100, when any horizontal spatial derivatives have been computed using centred finite differencing across about 200km; this compromises between brevity and precision, and allows for semi-systematic increases occurring in certain values, such as vorticity, if and when smaller gridlengths are utilised.

A few columns will be character-based, with an upper limit on character number of 6. ! will be the missing data indicator for character variables.

SIMPLIFIED EXAMPLE: (data file with two auxiliary header files - 'column title' and 'scaling information' - concatenated on top):

Model	Date	Time	LeadTime	Region	Lat	Lon	MSLP
L=LAM	dd/mm/yy	Hours*1	Hours*1		Deg*10	Deg*10	Mb
L	14/01/98	6	0	A	515	-10	1000
L	14/01/98	9	3	A	525	-5	996
L	14/01/98	12	3	A	600	-120	99999

A real file will contain many more columns than this example.

2) Variables

The table below lists variables that will be stored in the database, for each frontal wave. Three variable types are indicated; N=numerical variable, C*? indicates character variable, with ? characters, and D indicates a dd/mm/yy date-format numerical variable. This date format is suited to Windows database/statistical packages such as Excel and Statgraphics. Some date information is 'duplicated' in a Year 2000-compliant format (end of table).

Basic variables are shown in normal font, ***supplementary*** variables in bold. Row shading pertains to document(s) which reference the quoted variables as follows:

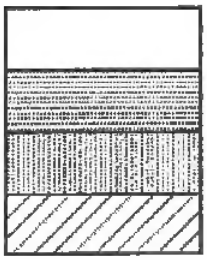

Self-explanatory or see Panagi and Dicks (1997)

Hewson (1997) and this document (including Appendices)

Hewson (1998)

Renfrew et al (1996)

	Column Heading	Standard Symbol	Description	Var Type	Units and Scaling, or †nature of char. entry
1	Model	-	Version of Met Office Unified Model	C*2	†e.g. L1
2	Region	-	Region used in frontal wave analysis	C*2	†e.g. D1
3	Resoln	-	Typical horizontal resolution of input data	N	Km *1
4	ProjWind	-	Projection information for interpreting vector and other 'x' and 'y' components	C*6	†e.g. PS20W
5	AnDate	DT	Date of analysis	D	dd/mm/yy
6	AnWkDay	-	Day of week for analysis	C*2	†e.g. MO
7	AnTime	DT	Time of analysis	N	Hrs *1
8	AcDate	VT	Validating date of data	D	dd/mm/yy
9	AcWkDay	-	Validating day of week of data	C*2	†e.g. MO
10	AcTime	VT	Validating time of data	N	Hrs *1
11	LeadTime	-	Difference of forecast time from analysis time (total hrs)	N	Hrs *1
12	Lat	ϕ	Latitude of frontal wave (+=N)	N	Deg *10
13	Lon	λ	Longitude of frontal wave (+=E)	N	Deg *10
14	WavType	-	Actual wave or Potential wave (section 4 and 5 above)	C*1	†A or P
15	WavStren	-	Standard or Weak wave (section 4 above)	C*1	†S or W
16	WaveErr	δc_{wave}	Frontal wave location error (as Hewson(97))	N	Km -1

17	WavFType		Warm front wave or Cold front wave (Appendix 5)	C*1	†W or C
18	MSLP	P	Mean sea level pressure	N	hPa *10
19	MSLPtype	-	Raw MSLP or derived from 1000mb height?	C*1	†R or H
20	RVor1	ξ	Relative Vorticity at 1km	N	s^{-1} *10^6
21	RVor1XF	-	Relative vorticity of the cross-front wind at 1km (Appendix 3)	N	s^{-1} *10^6
22	RVor1LF	-	Relative vorticity of the along-front wind at 1km (Appendix 3)	N	s^{-1} *10^6
23	GRVor1	ξ_G	Geostrophic Relative Vorticity at 1km	N	s^{-1} *10^6
24	GRVor1XF	-	Relative vorticity of the cross-front geostrophic wind at 1km (Appendix 3)	N	s^{-1} *10^6
25	GRVor1LF	-	Relative vorticity of the along-front geostrophic wind at 1km (Appendix 3)	N	s^{-1} *10^6
26	FX	n_x	x-component of the along-front unit vector (Eq A1.5, Appendix 1)	N	*10^5
27	FY	n_y	y-component of the along-front unit vector (Eq A1.6, Appendix 1)	N	*10^5
28	Te9	T	Temperature at 900mb	N	°C *10
29	ThW9	θ_{w900}	Theta-W at 900mb	N	°C *10
30	ThW7	θ_{w700}	Theta-W at 700mb	N	°C *10
31	ThW5	θ_{w500}	Theta-W at 500mb	N	°C *10
32	Th9	θ_{900}	Potential Temperature at 900mb	N	°C *10
33	Th7	θ_{700}	Potential Temperature at 700mb	N	°C *10
34	Th5	θ_{500}	Potential Temperature at 500mb	N	°C *10
35	ABZGrThW	$\lvert\nabla\theta_w\rvert_{ABZ}$	Theta-W gradient in the adjacent baroclinic zone at 1km	N	°C/km *10^4
36	AFGrThW	$\nabla\theta_w \cdot \hat{\mathbf{n}}$	Along-front Theta-W gradient at 1km	N	°C/km *10^4
37	Fr600ThW	(Appendix 6)	Value of Theta-W front locating diagnostic at 600mb	N	°C/Km^2 *10^8
38	GThWAdv6	$-\mathbf{V}_G \cdot \nabla\theta_w$	Geostrophic advection of Theta-W at 600mb	N	°C/s *10^6
39	ABZGrTh	$\lvert\nabla\theta\rvert_{ABZ}$	Theta gradient in the adjacent baroclinic zone at 1km	N	°C/km *10^4
40	AFGrTh	$\nabla\theta \cdot \hat{\mathbf{n}}$	Along-front Theta gradient at 1km	N	°C/km *10^4
41	Fr600Th	(Appendix 6)	Value of Theta front locating diagnostic at 600mb	N	°C/Km^2 *10^8
42	GThAdv6	$-\mathbf{V}_G \cdot \nabla\theta$	Geostrophic advection of Theta at 600mb	N	°C/s *10^6
43	U7	U_{700}	U Component at 700mb	N	m/s *10
44	V7	V_{700}	V component at 700mb	N	m/s *10
45	U5	U_{500}	U Component at 500mb	N	m/s *10
46	V5	V_{500}	V component at 500mb	N	m/s *10
47	U3	U_{300}	U Component at 300mb	N	m/s *10

48	V3	V_{300}	V component at 300mb	N	m/s *10
49	PV1km	-	PV at 1km	N	PVunits *100
50	PV2ht	-	Height of PV2 surface (scan down)	N	dm
51	PVfold	-	Whether fold exists in surface of PV=1.5 PV units	C*1	Y or N
52	W9	ω_{900}	Model Vertical velocity at 900mb	N	cm/s *100
53	W7	ω_{700}	Model Vertical velocity at 700mb	N	cm/s *100
54	W5	ω_{500}	Model Vertical velocity at 500mb	N	cm/s *100
55	Div1000	$\nabla\cdot V_{1000}$	Divergence at 1000mb	N	s^{-1} *10^7
56	Div900	$\nabla\cdot V_{900}$	Divergence at 900mb	N	s^{-1} *10^7
57	Div800	$\nabla\cdot V_{800}$	Divergence at 800mb	N	s^{-1} *10^7
58	Div500	$\nabla\cdot V_{500}$	Divergence at 500mb	N	s^{-1} *10^7
59	Div300	$\nabla\cdot V_{300}$	Divergence at 300mb	N	s^{-1} *10^7
60	LandSea	-	Whether nearest gridpoint is land or sea	C*1	†L or S
61	SeaGrPts	-	Number of the 9 adjacent gridpoints which are sea	N	*1
62	SST	T_{surf}	Land/Sea Surface Temperature at nearest grid point	N	°C *10
63	GrSST	$\lvert\nabla T_{surf}\rvert$	Gradient of Land/Sea Surface Temperature	N	°C/km *10^4
64	GrSSTx	$\partial T_{surf}/\partial x$	'X'-component of the Land/Sea Surface Temperature gradient	N	°C/km *10^4
65	GrSSTy	$\partial T_{surf}/\partial y$	'Y'-component of the Land/Sea Surface Temperature gradient	N	°C/km *10^4
66	AlphaMin	α_{min}	Critical environmental strain threshold (Appendix 3)	N	s^{-1} *10^7
67	VortMeth		Method by which vorticity values (eg. vars 20-22) were calculated (Appendix 3)	C*6	e.g. OIGFLG
68	UE	U_E	U component of the environmental wind	N	m/s *10
69	VE	V_E	V component of the environmental wind	N	m/s *10
70	dVEdS	$\partial V_{Es}/\partial s$	Rate of change of the front-parallel component of the environmental wind in a front-parallel direction	N	s^{-1} *10^7
71	dVEdN	$\partial V_{Es}/\partial n$	Rate of change of the front-parallel component of the environmental wind in a front-normal direction	N	s^{-1} *10^7
72	RH9	-	Relative humidity w.r.t. ice at 900mb	N	% *10
73	RH7	-	Relative humidity w.r.t. ice at 700mb	N	% *10
74	RH5	-	Relative humidity w.r.t. ice at 500mb	N	% *10
75	WQGT7	ω_{qg7}	Vertical velocity at 700mb attributable to q-g forcing	N	cm/s *100
76	WQGU7	ω_{qgu7}	Vertical velocity at 700mb attributable to q-g forcing above 650mb	N	cm/s *100

77	WQGM7	ω_{qgm7}	Vertical velocity at 700mb attributable to q-g forcing between 850mb and 550mb	N	cm/s *100
78	WQGL7	ω_{qgl7}	Vertical velocity at 700mb attributable to q-g forcing below 750mb	N	cm/s *100
79	THIKN05	Z_T	1000-500mb thickness	N	dm *10
80	ShRVort3	ζ_{sh}	Shear relative vorticity at 300mb	N	$s^{-1}*10^5$
81	GOcRate1	χ_G	Geostrophic rate of occlusion at 1km, n=4, R=100km (Appendix 4)	N	$s^{-1}*10^6$
82	GOcRate2	χ_G	Geostrophic rate of occlusion at 1km, n=4, R=200km (Appendix 4)	N	$s^{-1}*10^6$
83	AnDay	-	Date (day) of analysis	N	*1
84	AnMonth	-	Month of analysis	N	*1
85	AnYear	-	Year of analysis (4 digit)	N	*1 (e.g. 2000)

Table 1: The contents of the frontal wave database

The potential use of most of these variables should be clear. Others require some explanation. For example the values/signs of variables 37 and 38 should allow the relative positions of upper objective fronts to be deduced; this is likely to relate to the stage of development of the wave. Similarly, the sign of variable 80 allows one to infer whether the frontal wave is on the poleward or equatorward side of any upper level jet stream.

7. Data Storage

If one allows for there being about 20 frontal waves in total (includes weak and potential waves) at any analysis or forecast time, and a total of about 85 variables, then frontal wave data for a full 48-hour LAM forecast for the north Atlantic area to be used in stages (1) and (2) (section 3) will occupy about 140,000 bytes. Similarly, one weeks worth of data, comprising one 48-hour forecast per day, plus a set of analysis files, would take up about 1.5Mbyte. A global dataset, as proposed in stage (3) of section 3, for one week, for similar resolution, would occupy of order 15Mbytes.

Appendix 1: The vorticity of the cross-front geostrophic wind

This Appendix relates masking inequality **[M3]** in Hewson(1997), that is the wave / anti-wave discriminant, to the sign of the relative vorticity of the cross-front geostrophic wind. **[M3]** is:

$$\left[\nabla|\nabla\tau|\times\hat{\mathbf{k}}\right]\cdot\left[\nabla[-\mathbf{V}_G\cdot\nabla\tau]\right] > 0$$

where τ is the surrogate for a thermodynamic variable, usually wet-bulb potential temperature, $\mathbf{V_G}$ is geostrophic wind, and ∇ is a horizontal or pressure-level gradient operator. Provided $|\nabla\tau|>0$ everywhere then the contour field of $(-\mathbf{V_G}.\nabla\tau=0)$ will be identical to the contour field of $((-\mathbf{V_G}.\nabla\tau)/|\nabla\tau|=0)$. Thus the vectors $\nabla(-\mathbf{V_G}.\nabla\tau)$ and $\nabla((-\mathbf{V_G}.\nabla\tau)/|\nabla\tau|)$ will be unidirectional wherever $-\mathbf{V_G}.\nabla\tau=0$ (which includes the tips of all waves and anti-waves). Thus (by also dividing throughout by $|\nabla|\nabla\tau||$) **[M3]** can be re-written as:

$$\frac{\left[\nabla|\nabla\tau|\times\hat{\mathbf{k}}\right]}{\left|\nabla|\nabla\tau|\right|}\cdot\nabla\left[\frac{-\mathbf{V_G}\cdot\nabla\tau}{|\nabla\tau|}\right] > 0 \qquad \textbf{(A1.1)}$$

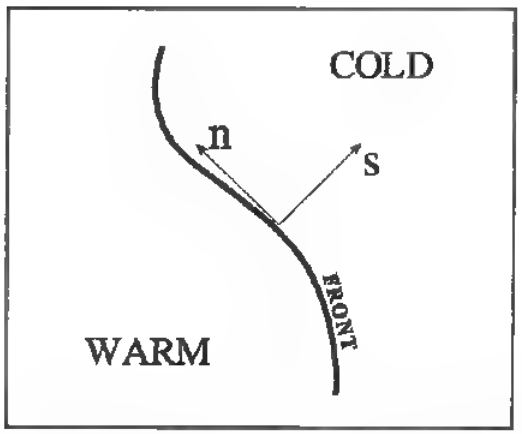

Figure A1.1: definition of a local front-relative co-ordinate system (*s,n*), as in Hewson (1998).

Now $\hat{\mathbf{s}}$ and $\hat{\mathbf{n}}$ are, respectively, the cross- and along-front unit vectors of a locally defined front-relative co-ordinate system (*s,n*) (Figure A1.1). They are given by:

$$\hat{\mathbf{s}} = \frac{\nabla|\nabla\tau|}{\left|\nabla|\nabla\tau|\right|} \qquad \text{and} \qquad \hat{\mathbf{n}} = -\hat{\mathbf{s}}\times\hat{\mathbf{k}}$$

Also, if there is no along front-thermal gradient, which is a good approximation at the tips of frontal waves and frontal anti-waves, then

$$\hat{\mathbf{s}} = -\frac{\nabla\tau}{|\nabla\tau|}$$

Thus equation (A1.1) can be reduced to

$$\left(-\hat{\mathbf{n}}\cdot\nabla[\mathbf{V_G}\cdot\hat{\mathbf{s}}]\right) > 0$$

That is:

$$(-\hat{\mathbf{n}})\cdot\left[\hat{\mathbf{s}}\frac{\partial(\mathbf{V_G}\cdot\hat{\mathbf{s}})}{\partial s}+\hat{\mathbf{n}}\frac{\partial(\mathbf{V_G}\cdot\hat{\mathbf{s}})}{\partial n}\right] > 0$$

Thus

$$\left(-\frac{\partial(\mathbf{V_G}\cdot\hat{\mathbf{s}})}{\partial n}\right) > 0 \qquad \text{or} \qquad \left(-\frac{\partial V_{Gs}}{\partial n}\right) > 0$$

where V_{Gs} is the local cross-front geostrophic wind. The bracketed quantities here thus represent 'the relative vorticity of the local cross-front geostrophic wind', or $\xi_{G(\text{cross-front-wind})}$. Note also that the full geostrophic relative vorticity, ξ_G, can be written as:

$$\xi_G = \xi_{G(\text{along front-wind})} + \xi_{G(\text{cross-front-wind})} = \frac{\partial V_{Gn}}{\partial s} - \frac{\partial V_{Gs}}{\partial n} \qquad \textbf{(A1.2)}$$

where, similarly, $\xi_{G(\text{along front wind})}$ is 'the relative vorticity of the local along-front, or front-parallel, geostrophic wind'.

Appendix 2: Identifying 'potential waves'

This Appendix describes the rationale for identifying 'potential (frontal) waves'. If an experienced forecaster or synoptician were presented with the isobars and fronts shown on Figure A2.1 and asked to identify regions in which frontal waves seemed to be most likely to develop, they would almost certainly select the locations marked 'C_w' and 'C_c', on account of weaknesses in the isobaric patterns nearby. These weaknesses are really areas where there is a local increase

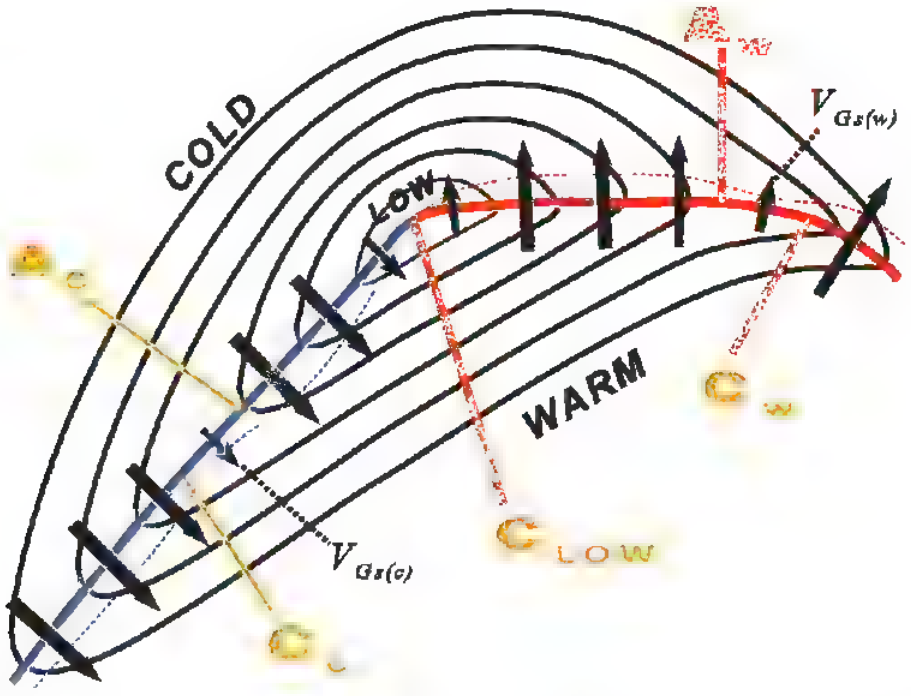

Figure A2.1 Schematic representation of an idealised mid latitude depression (marked C_{LOW}). Thin black lines are isobars (omitted around edges); thick red and blue lines are warm and cold fronts respectively. Thin dashed red and blue lines show approximate frontal positions a short time later (system-relative frame). The two airmasses are labelled. Arrows represent cross-front geostrophic wind components. Letters C_C and C_W denote potential (frontal) waves, letters A_C and A_W potential anti-waves (see text).

in the along-front isobaric spacing, or equivalently a local reduction in the cross-front geostrophic wind (V_{Gs} in Appendix 1 terminology). Vectors of V_{Gs}, as deduced from the isobaric spacing, are shown on the Figure. *Small changes* to either of the smaller vectors labelled $V_{Gs(w)}$ and $V_{Gs(c)}$ could change the *signs* of those winds, in which case the warm front segment bounded approximately by points A_w and C_w would change to a cold front, or the cold front segment bounded

approximately by points A_c and C_c would change to a warm front. If this happened then we would have a true frontal wave at C_w (or C_c) and a true anti-wave at A_w (or A_c), because true frontal waves and anti-waves lie at cold/warm front meeting points. So because only small wind changes are required near C_w and C_c on Figure A2.1 to produce real frontal waves, we can say that these points represent 'potential (frontal) waves' (and A_w and A_c 'potential anti-waves'). Also, if one considers advecting the fronts, for a small timestep, according to the cross-front winds V_{Gs} shown, then it is clear that small ripples, or changes in orientation, would develop on both the warm front and the cold front, close to the vectors $V_{Gs(w)}$ and $V_{Gs(c)}$, as shown by the thin dashed lines. Such ripples also hint at possible wave development.

What is required now is a mathematical method for objectively pinpointing potential waves that is consistent with the synoptic practice referred to above, simple to apply and dynamically correct. Such a method should be based on V_{Gs}. Consider the relative vorticity of this wind, $\xi_{G(\text{cross-front-wind})}$. There are three places on the front where this clearly reaches a maximum, that is to say there are three places where there is a maximum cyclonic rotation of V_{Gs}. These are C_w and C_c (the potential waves) and 'C_{LOW}' (a true wave, or depression). Similarly there are two places where there is a maximum in anticyclonic rotation of V_{Gs}; these are A_w and A_c, the 'potential anti-waves'. Thus, as the five A and C locations all represent turning points, in the along-front direction, of the variable $\xi_{G(\text{cross-front-wind})}$, they can be mathematically identified by the following diagnostic:

$$\frac{\partial \xi_{G(\text{cross-front-wind})}}{\partial n} = 0 \qquad \text{or} \qquad \frac{\partial^2 V_{Gs}}{\partial n^2} = 0 \qquad \textbf{[L3]}$$

By combining **[L3]** with **[L1]**, **[M1]** and **[M2]** in Hewson (1998), which together defined an objective front, we now have a mathematical definition which encompasses both potential waves and potential anti-waves. By then adding a criterion that states that the vorticity of the cross front wind must be greater than zero, ie **[M3]** (see Appendix 1), we will successfully eliminate all the 'potential anti-waves'.

If one accepts that frontal waves, and thus potential waves, are characterised by cyclonic rotation of their fronts, and that, to a good first approximation this rotation can be attributed to 'geostrophic frontal advection', then the definition that has been given can be considered dynamically correct (note how frontal segments near to both C_w and C_c on Figure A2.1 undergo slight cyclonic rotation as they move towards the positions shown by thin dashed lines). One might wish to use the full geostrophic relative vorticity instead of the vorticity of the cross-front geostrophic wind in the computation; however this would have the disadvantage of being 'contaminated' by the along front wind, V_{Gn}, which should have no direct impact on frontal rotation.

There remains one problem. This is that the main low centre on the example in Figure A2.1 will have been identified as both a true frontal wave and a potential frontal wave. One could use searching algorithms to avoid this 'double counting'. However, a better and more complete solution is to use one additional diagnostic, in the definition of a potential wave, that will have the effect of excluding those which are 'also' true waves. The main difference between waves and potential waves (so far) is that the geostrophic thermal advection is only zero at a true wave. However it would be difficult to utilise this in practice because, due to the graphical interpolation, most potential waves that are really replicating a true wave will not coincide *exactly* with where the geostrophic thermal advection is zero. A more reliable method can be deduced by referring

to Figure A2.1. Note that the sign of the scalar quantity V_{Gs} does not change, in the along-front direction, across C_c and C_w, but does change at 'C_{LOW}'. Therefore:

$$\text{At } C_c \text{ and } C_w \quad \left|\frac{\partial|V_{Gs}|}{\partial n}\right| = \left|\frac{\partial V_{Gs}}{\partial n}\right|, \qquad \text{whilst at } C_{LOW} \quad \left|\frac{\partial|V_{Gs}|}{\partial n}\right| \ll \left|\frac{\partial V_{Gs}}{\partial n}\right|$$

So a suitable criterion to complete the definition of a potential frontal wave (along with **[L1]**, **[L3]**, **[M1]**, **[M2]** and **[M3]**) is:

$$\left|\frac{\partial|V_{Gs}|}{\partial n}\right| \Bigg/ \left|\frac{\partial V_{Gs}}{\partial n}\right| \geq K_4 \qquad \textbf{[M 4]}$$

where K_4 is the masking criterion threshold. Tuning will be required to find an appropriate value for K_4, to accommodate rounding errors and the effects of interpolation, but it is likely to be just less than 1.

Note also that the sign of the geostrophic thermal advection (diagnostic in **[L2]**) allows one to discriminate between potential warm front waves and potential cold front waves (Appendix 5).

Appendix 3: Critical strain threshold and intrinsic frontal vorticity

Bishop & Thorpe (1994) and Renfrew et al (1997) indicate that there is a theoretical threshold value (α_{min}), for the along-front strain of the horizontal environmental flow field, in the vicinity of a front, above which wave growth, on that front, will be suppressed. By assuming that the absolute vorticity in the general frontal environment, but remote from the front itself, can be approximated by f (the Coriolis parameter) equation (5.7) in Bishop & Thorpe (1994) reduces to:

$$\alpha_{min} = \left(\frac{f}{4}\right)\left(\frac{\xi_{Front}}{\xi_{Front} + f}\right) e^{\left(-2\pi\frac{W}{L}\right)} \qquad \textbf{(A3.1)}$$

where

W	is the width of the frontal strip,
L	is the length of the frontal strip,
ξ_{Front}	is the intrinsic relative vorticity of the frontal strip.

Now let:

$\xi_{Front(Model)X}$	be a model estimate of the intrinsic relative vorticity of the frontal strip computed using differencing method X,
$\xi_{Wave(Model)X}$	be a model estimate of the intrinsic relative vorticity of any wave or potential wave, computed using differencing method X,

$\xi_{(Model)X}$ be the full model relative vorticity, *at* the front, computed using differencing method X.

so that:

$$\xi_{(Model)X} = \xi_{Front(Model)X} + \xi_{Wave(Model)X}$$

In principle it should be reasonably straightforward to compute α_{min} in equation (A3.1) from gridded model data, by assuming that the hypothetical frontal wave with which we are dealing will have the structure of the most unstable unstrained barotropic normal mode, that is one for which (W/L) = 1/8. However we do not know ξ_{Front}.

In the first instance we can calculate $\xi_{(Model)X}$, but actually want to find a value for $\xi_{Front(Model)X}$ to provide an estimate of ξ_{Front}. We know that *for a straight 2-dimensional front* (i.e. no waves or potential waves) $\xi_{Wave(Model)X}=0$, and also that

$$\xi_{Front(Model)X} = \frac{\partial V_n}{\partial s} \qquad \textbf{(A3.2)}$$

which is the shear in the along-front (front-parallel) wind. If we then assume that, *for fronts in general,* the contribution of waves and potential waves to the shear in the along-front wind is relatively small, it follows that equation (A3.2) will in fact will hold for all fronts. Similarly,

$$\xi_{Wave(Model)X} = -\frac{\partial V_s}{\partial n} \qquad \textbf{(A3.3)}$$

which is the shear in the cross-front wind, will hold for all fronts. Investigation of a limited number of real cases suggests that waves or potential waves, on a front, do indeed make a relatively small contribution to the shear in the along-front wind, but even if this were not true equation (A3.2) would still give a better estimate than just using $\xi_{(Model)X}$. Thus we would recommend, in the first instance, using $\partial V_n/\partial s$ to provide an estimate of ξ_{Front} for equation (A3.1). Note that Renfrew et al (1997) use an along-front average of $\xi_{(Model)X}$; equation (A3.2) is providing an alternative which can be computed at individual gridpoints, and is thus more easily utilised for the frontal wave database.

It is important to now consider the impact of using different differencing methods (X) to compute $\xi_{Front(Model)X}$ in equation (A3.2). Note that the value of any gradient quantity, such as $\partial V_n/\partial s$, computed from gridded model data, depends on the following:

1) The basic model gridlength
2) The finite differencing scheme used
3) Interpolation before and/or after the computation

One would hope that the effect of varying these parameters would be small enough to be ignored. However across features which tend to exhibit a discontinuous structure, such as fronts, this is not true. As an example, consider, for a particular front, a model for which (i) gridlength is greater than the true distance across which the vector wind change occurs, and (ii) gridpoint values accurately represent the true winds. Then model values of $\xi_{Front(Model)X}$, derived using simple finite differencing techniques on gridpoint winds, will be inversely proportional to the lengthscale (d_X)

used in the computation, i.e.

$$\xi_{\text{Front(Model)X}} \propto \frac{1}{d_X} \qquad \text{(A3.2)}$$

This means (for example) that if one were to use first order centred finite differencing on a staggered grid, to compute $\xi_{\text{Frcat(Model)X}}$ between adjacent wind gridpoints, the values obtained would be twice those obtained if a non-staggered grid had been used. Thus the subscript 'X', representing the method of computation, is significant (variable 67 in the database will describe the method - for example 'O1CFLG' would indicate that 1st Order Centred Finite differencing had been applied on the Local Grid, ie the grid as represented by variables 1 to 4).

What is really required is an 'intrinsic model (frontal) relative vorticity'. This can only be computed with a full knowledge of the way in which the momentum equations are formulated within the model itself, and thus the method of computation may vary with model. Thus it is not possible to state here a method of computing ξ_{Front}, nor, therefore, α_{min}, which would be appropriate for all models and projections.

There are also a number of related theoretical questions to be addressed. Some are listed below ('mature fronts' here means fronts that possess a relatively discontinuous wind structure):

1) What is the smallest wavelength frontal wave that a particular model can be expected to represent well?
2) Should it be just waves of very small length scales that grow on mature fronts?
3) Do synoptic scale waves grow on mature fronts, and if so by what mechanism?
4) When assessing the importance of the along-front stretching as regards synoptic wave development should we be excluding non-mature fronts?

Whilst recognising that there are still a number of issues to be resolved, in the database we will be including, for convenience, 'trial' values for α_{min}. These will simply be derived on the basis of equation (A3.1), with $\partial V_n/\partial s$ substituted for ξ_{Front} and computed as indicated by variable 67.

Appendix 4: Geostrophic rate of occlusion

Although the structure and even the existence of occlusions has recently come under close scrutiny - as demonstrated by the development of conceptual models of cyclone evolution which incorporate warm and cold fronts but not occlusions (e.g. Shapiro & Keyser (1990) and Monk (1992)) - it should nevertheless be possible to develop a relatively uncontroversial method of computing the speed of rotation of a cold front relative to a warm front, and thence a nominal 'rate of occlusion' for a particular frontal wave or depression. Such a quantity is of interest because it relates to the rate at which the supply of warm low-level air within a weather system is being depleted, most probably through ascent. Such ascent can lead to rapid intensification of the system, particularly if it also involves the release of large amounts of latent heat. A large 'rate of occlusion' will only occur if there is considerable departure, in the wind structure around a low, from an axi-symmetric pattern, and it is probably no coincidence that major mid-latitude storms, such as the October storm of 1987 in Southern England (see Monk for this example and others), often possess a very non axi-symmetric structure in winds and mean sea level pressure, that is consistent with a rapid 'rate of occlusion', during and immediately after the periods when they

were developing most rapidly. Objective fronts can be used to enable the 'Geostrophic rate of occlusion' to be computed automatically as a diagnostic field as described below.

First we define the 'rate of occlusion', for a particular frontal wave or depression, to be:

> 'The difference between the warm front and the cold front angular velocities, estimated using the cross-front wind'

The sign convention is that the rate is positive if the cold front is tending to catch up the warm front. An identical definition of the 'rate of occlusion' is

> 'The average angular velocity, towards the warm air, of the (two) fronts, estimated using the cross-front wind'

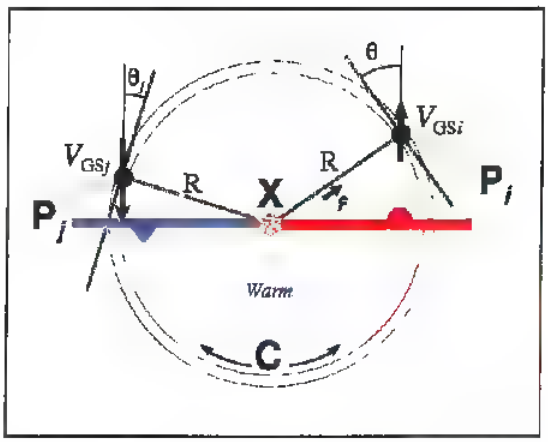

Figure A4.1 Schematic illustrating the methodology used in computing the 'geostrophic rate of occlusion' about a point X, as explained in the text. X is a wave tip, or depression centre, whilst red and blue lines are (objective) warm and cold surface fronts. C is a circle of radius R whose centre is X.

These two expressions clearly include the assumption that 'frontal advection' gives a good approximation to true frontal movement. We further refine this by utilising the (cross-front) *geostrophic* wind; this is consistent with standard synoptic practice, although it should be noted that we are *not* allowing for the (empirical) tendency of warm fronts to progress at slightly sub-geostrophic speeds (see, for example, Meteorological Office (1991)).

To simplify computation we now assume that the warm and cold fronts are parallel, as in Figure A4.1. With the above assumptions frontal rotation now depends only on the front-normal geostrophic wind, V_{Gs}. Then, from Figure A4.1, it is clear that the angular velocity (Ω_{GWi}) of the front, about X, towards the warm air, due to the front normal wind at P_i, is given by:

$$\Omega_{GWi} = -\frac{V_{Gsi}\cos\theta_i}{R} = -\frac{V_{Gsi}}{R}\left(\frac{\mathbf{V}_{Gsi}\cdot(\hat{\mathbf{r}}\times\hat{\mathbf{k}})}{|\mathbf{V}_{Gsi}}\right)$$

where $\hat{\mathbf{r}}$ is a unit radial vector as shown on the Figure. Then the geostrophic rate of occlusion (γ_G), about a wave tip X, is given by the average value, for all points P_i around a circle centred on X (such as C on Figure A4.1) of Ω_{GWi}. That is:

$$\gamma_G = \frac{-1}{nR}\sum_{i=1}^{n} V_{Gsi}\left(\frac{\mathbf{V}_{Gsi}\cdot(\hat{\mathbf{r}}\times\hat{\mathbf{k}})}{\mathbf{V}_{Gsi}}\right) \qquad \textbf{(A4.1)}$$

where $n \geq 3$ and all points P_i are equally spaced around C. In practice the size of the circle C should be of the same order as the systems in question, say R ~ 50-500km to produce meaningful results.

When using a simple non-staggered polar stereographic grid the computation is straightforward. One can use n=4 and R=gridlength in equation (A4.1), so that the summation at

The discussion above pertains only to true frontal waves. Because potential waves do not coincide with a point at which there is zero geostrophic cross-front wind, the concept of 'rate of occlusion' for such features is arguably rather ill-defined. So whilst it is possible to calculate γ_G at all points in space, the values attained in the vicinity of potential waves are probably not meaningful. An alternative might have been to use a quantity related to $\partial^2 V_{GS} / \partial n^2$ except that that is, by definition, zero at a potential frontal wave (Appendix 2).

Appendix 5: Type of Wave

In Appendix 2 it was indicated that the sign of the geostrophic thermal advection at the tip of a potential wave indicates whether that wave is a potential warm front wave or a potential cold front wave. This methodology will not work for true objective frontal waves because they are situated where the geostrophic thermal advection is zero. One might then wish to use the history of such features as an alternative. On Figure 4, for example, both of the new waves on the lower panels could be described as warm front waves, because they originated from potential warm front waves (upper panels). However such an approach would involve tracking lows, which is complex, and inconsistent with the structure of the database as described in this document. A suitable alternative is to use the sign of the 'geostrophic rate of occlusion', γ_G, (Appendix 4), as the discriminant. Those true waves located where γ_G is positive will be cold front waves, and those located where γ_G is negative will be warm front waves. This can be explained by reference to Figure A2.1. Consider adding small, additional, symmetrical cyclonic perturbations to the geostrophic cross-front winds near the points labelled C_C and C_W on Figure A2.1, such that the lighter winds just reverse sign. This emulates the development of true cold and warm front waves respectively. Now estimate average values of Ω_{GWi} at the labelled points (equation A4.1 in Appendix 4), for a radial distance equal to half the vector spacing. At C_C, because V_{GS} is on average negative, γ_G will be positive, consistent with a cold front wave. The opposite applies at C_W. This also hints at why warm front waves tend to be less developmental than cold front waves.

Table A5.1 summarises how waves will be categorised in the frontal wave database.

	'Warm Front Wave'	'Cold Front Wave'
Potential Frontal Wave	Geostrophic thermal advection at wave tip is positive	Geostrophic thermal advection at wave tip is negative
True frontal wave	Geostrophic rate of occlusion at wave tip is negative	Geostrophic rate of occlusion at wave tip is positive

Table A5.1: The means by which waves will be categorised as warm front waves or cold front waves.

Acknowledgements

Thanks to Andy White, Craig Bishop, Alan Thorpe, Ian Renfrew and Sid Clough for providing helpful feedback on the contents of this document.

References

Bishop, C.H. and Thorpe, A.J. (1994). Frontal Wave Stability during Moist Deformation Frontogenesis. Part II: The Suppression of Nonlinear Wave Development. *J. Atmos. Sci.*, **51**, 874-888.

Hewson, T.D. (1998). Objective Fronts. *Meteorol. Appl.* **5**. 37-65.

Hewson, T.D. (1997). Objective Identification of Frontal Wave Cyclones. *Meteorol. Appl.* **4**. 311-315.

Joly, A., Jorgensen, D., Shapiro, M. A., Thorpe A. J., Bessemoulin, P., Browning, K. A., Cammas, J. P., Chalon, J. P., Clough, S. A., Emanuel, K. A., Eymard, L., Gall, R., Hildebrand, P. H., Langland, R. H., Lemaître, Y., Lynch, P., Moore, J. A., Persson, P. O. G, Snyder, C. & Wakimoto, R. M. (1997). The Fronts and Atlantic Storm-Track Experiment (FASTEX): Scientific objectives and experimental design. *Bull. Am. Meteorol. Soc.*, **78**, 1917-1940.

Kurz, M. (1995). Synoptic-scale waves. In 'Images in weather forecasting'. Cambridge University Press. Editors M.J.Bader, G.S.Forbes, J.R.Grant, R.B.E.Lilley, A.J.Waters. 187-205.

Meteorological Office. (1991). Meteorological Glossary. London. HMSO, 335pp.

Monk, G. A. (1992). Synoptic and mesoscale analysis of intense mid-latitude cyclones. *Meteorol. Mag.*, **121**: 269-283.

Panagi, P. & Dicks, E. (1997). Met. Office Unified Model data, diagnostic graphics programs, and other observational data available from the JCMM through the aegis of the Universities Weather Research Network UWERN. JCMM internal report no 69. Department of meteorology, Reading university.

Renfrew, I.A., Thorpe, A.J., and Bishop, C.H. (1997). The role of the environmental flow in the development of secondary frontal cyclones. *Q.J.R.Meteorol.Soc.* **123**. 1653-1675.

Shapiro, M. A. & Keyser, D. (1990). Fronts, Jet Streams and the Tropopause; in 'Extratropical Cyclones, The Erik Palmén Memorial Volume'. American Meteorological Society, Boston. 167-191.

Van Der Wal, A. & Milton, S.F. (1998) The Prediction of Extratropical Cyclones and Blocking in the U.K. Meteorological Office Global N.W.P. Model. Submitted to *Meteorol. Appl.* January 1998. 16pp.

JCMM. 14/4/98. Tim Hewson.

CURRENT JCMM INTERNAL REPORTS

This series of JCMM Internal Reports, initiated in 1993, contains unpublished reports and also versions of articles submitted for publication. The complete set of Internal Reports is available from the National Meteorological Library on loan, if required.

1. **Research Strategy and Programme**
   K A Browning et al
   January 1993

2. **The GEWEX Cloud System Study (GCSS)**
   GEWEX Cloud System Science Team
   January 1993

3. **Evolution of a mesoscale upper tropospheric vorticity maximum and comma cloud from a cloud-free two dimensional potential vorticity anomaly**
   K A Browning
   January 1993

4. **The Global Energy and Water Cycle**
   K A Browning
   July 1993

5. **Structure of a midlatitude cyclone before occlusion**
   K A Browning and N Roberts
   July 1993

6. **Development in Systems and Tools for Weather Forecasting**
   K A Browning and G Szejwach
   July 1993

7. **Diagnostic study of a narrow cold frontal rainband and severe winds associated with a stratospheric intrusion**
   K A Browning and R Reynolds
   August 1993

8. **Survey of perceived priority issues in the parametrizations of cloud-related processes in GCMs**
   K A Browning
   September 1993

9. **The Effect of Rain on Longwave Radiation**
   I Dharssi
   September 1993

10. **Physical Cloud Microprocesses - A Description of the Parametrization used in the Large Eddy Model**
    H Swann
    July 1994

11. **An Appreciation of the Meteorological Research of Ernst Kleinschmidt**
    A J Thorpe
    May 1992

12. **Potential Vorticity of Flow Along the Alps**
    A J Thorpe, H Volkert and Dietrich Heimann
    August 1992

13. **The Representation of Fronts**
    A J Thorpe
    January 1993

14. **A Parametrization Scheme for Symmetric Instability: Test for an Idealised Flow**
C S Chan and A J Thorpe
February 1993

15. **The Fronts 92 Experiment: a Quicklook Atlas**
Edited by T D Hewson
November 1993

16. **Frontal wave stability during moist deformation frontogenesis**
Part 1. Linear wave dynamics
C H Bishop and A J Thorpe
May 1993

17. **Frontal wave stability during moist deformation frontogenesis**
Part 2. The suppression of non-linear wave development
C H Bishop and A J Thorpe
May 1993

18. **Gravity waves in sheared ducts**
C Bishop and A J Thorpe
November 1993

19. **Potential Vorticity and the Electrostatics Analogy: Quasi-Geostrophic Theory**
C Bishop and A J Thorpe
November 1993

20. **Recent Advances in the Measurement of Precipitation by Radar**
A J Illingworth
April 1993

21. **Micro-Physique et Givrage. Cloud Microphysics and Aircraft Icing**
A J Illingworth
May 1993

22. **Differential Phase Measurements of Precipitation**
M Blackman and A J Illingworth
May 1993

23. **Estimation of Effective Radius of Cloud Particles from the Radar Reflectivity**
N I Fox and A J Illingworth
May 1993

24. **A Simple Method of Dopplerising a Pulsed Magnetron Radar**
A Hau, A J Illingworth and J Eastment
November 1993

25. **Radiation and Polar Lows**
George C Craig
February 1994

26. **Collected preprints submitted to the International Symposium on the Life Cycles of Extratropical Cyclones; Bergen, Norway, 27 June - 1 July 1994**
April 1994

27. **Convective Frontogenesis**
Douglas J Parker and Alan J Thorpe
April 1994

28. **Improved Measurement of the Ice Water Content in Cirrus Using a Total Water Evaporator**
Philip R A Brown and Peter N Francis
April 1994

29. **Mesoscale Effects of a Dry Intrusion within a Vigorous Cyclone**
K A Browning and B W Golding
April 1994

30. **GEWEX Cloud System Study, Science Plan**
May 1994

31. **Parametrization of Momentum Transport by Convectively Generated Gravity Waves**
R Kershaw
February 1995

32. **Mesoscale Modelling Newsletter No 5**
May 1994

33. **Observations of the mesoscale sub-structure in the cold air of a developing frontal cyclone**
K A Browning, S A Clough, C S A Davitt, N M Roberts and T D Hewson
May 1994

34. **Longwave Radiative Forcing of a Simulated Tropical Squall Line**
Imtiaz Dharssi
July 1994

35. **On the nature of the convective circulation at a kata-cold front**
K A Browning
September 1994

36. **Collective preprints of papers submitted to the COST-75 International Seminar on Advanced Weather Radar Systems, Brussels, 20-23 September 1994**
November 1994

37. **Use of satellite imagery to diagnose events leading to frontal thunderstorms: Parts 1 and 11 of a case study**
K A Browning and N M Roberts
November 1994

38. **The role of spaceborne millimetre-wave radar in the global monitoring of ice cloud**
P R A Brown, A J Illingworth, A J Heymsfield, G M McFarquahar, K A Browning and M Gosset
December 1994

39. **Potential Vorticity Inversion**
Michael Ziemianski
October 1994

40. **Theory of mature tropical cyclones; a comparison between Kleinschmidt (1951) and Emanuel (1986)**
Suzanne L Gray
December 1994

41. **Dispersion and removal of pollutants during the passage of an atmospheric frontal system**
N R Gimson
December 1994

42. **The role of snow sublimation in frontogenesis**
D J Parker and A J Thorpe
December 1994

43. **Potential vorticity and the electrostatics Analogy: Ertel-Rossby formulation**
A J Thorpe and C H Bishop
December 1994

44. **Mesoscale aspect of extratropical cyclones: an observational perspective**
K A Browning
January 1995

45. **A Polar Low Outbreak: Evolution and Mesoscale Structures**
T D Hewson, G C Craig and C Claud
February 1995

46. **Generation of near-surface gusts of deep convection**
K Nakamura and R Kershaw
April 1995

47. **Attribution Concepts applied to the Omega Equation**
S A Clough, C S A Davitt and A J Thorpe
June 1995

48. **Parametrization of mixed-phase cloud and precipitation**
Susan P Ballard and M Gerard Hutchinson
June 1995

49. **Short-range forecasting of stratocumulus: Initialization Prediction**
Susan Ballard, Simon D Jackson and B Macpherson
June 1995

50. **Contributions of the JCMM/Dept of Meteorology Radar Group to the 27th AMS Radar Meteorology Conference, Vail October 1995**
June 1995

51. **Cold Pools in Shear**
Douglas J Parker
September 1995

52. **High-resolution analysis of frontal fracture**
K A Browning, S P Ballard and C S A Davitt
September 1995

53. **The Albedo of Broken Cloud Fields: Calculations using a modified two stream radiation code**
Imtiaz Dharssi and Roy Kershaw
October 1995

54. **Parametrization of momentum transport by convection. I: Theory and cloud modelling results**
R Kershaw and D Gregory
November 1995

55. **Variation of frontal structure along a cold front**
K A Browning and N M Roberts
November 1995

56. **Secondary Frontal Waves**
Douglas Parker
December 1995

57. **Objective Fronts**
T D Hewson
March 1996

58. **Mesoscale analysis of the activation of a cold front during cyclogenesis**
K A Browning, N M Roberts and A J Illingworth
June 1996

59. **Investigation of Different Representations of Rain in a 1-d Evaporation Model**
H Swann
May 1996

60. **Parametrization of diabatic processes in the inversion of the omega-equation**
M Athanassiadou and A J Thorpe
June 1996

61. **The Role of the Environmental Flow in the Development of Secondary Frontal Cyclones**
I A Renfrew, A J Thorpe and A Joly
June 1996

62. **Consequences of the geostrophic momentum approximation on barotropic instability**
S Malardel, A J Thorpe and A Joly
June 1996

63. **Contributions to the AMS/RMS Conference on Mesoscale Processes**
Reading, 9-13 September 1996

64. **Vorticity and Potential Vorticity in Stratified Flows Interacting with an Isolated Obstacle**
Jorge A Gutiérrez and A J Thorpe
September 1996

65. **Triple Point Development: Two Case Studies**
Douglas Parker
September 1996

66. **Radar observations of wind-shear splitting within evolving atmospheric Kelvin-Helmholtz billows**
D Chapman and K A Browning
April 1997

67. **Cold Frontal Structure derived from radar wind profilers**
K A Browning, D Jerrett, J Nash, T Oakley, N M Roberts
May 1997

68. **The dry intrusion and its effect on the frontal, cloud and precipitation structure of extratropical cyclones**
K A Browning - Text of invited special lecture at the Spring Conference
of the Meteorological Society of Japan, University of Tsukuba, 22 May 1997

69. **Met. Office Unified Model data, diagnostic graphics programs, and other observational data available from the JCMM through the aegis of the Universities Weather Research Network (UWERN).** (Plus supplement)
Peter Panagi and Ed Dicks
June 1997

70. **Contributions of the JCMM/Dept of Meteorology Radar Group to 28th AMS Radar Meteorology Conference.** Austin, Texas
September 1997

71. **Sensitivity of short-range weather forecasts to local potential vorticity modifications**
Meral Demirtas and Alan Thorpe
July 1997

72. **Objective identification of frontal wave cyclones**
T D Hewson
August 1997

73. **Attribution and its application to mesoscale structure associated with tropopause folds**
A J Thorpe
September 1997

74. **The Role of the Environmental Flow in the Development of Secondary Frontal Cyclones**
Ian A Renfrew, Alan J Thorpe and Craig H Bishop
September 1997

75. **Potential Vorticity: A short history of its definitions and uses**
Alan J Thorpe and Hans Volkert
September 1997

76. **Superposing Semi-Geostrophic Potential Vorticity Anomalies**
H R Birkett and A J Thorpe
September 1997

77. **Short period forecasting of catchment-scale precipitation.**
Part 1: the role of Numerical Weather Prediction
M A Pedder, M Haile and A J Thorpe
September 1997

78. **Verification of the Tracking Technique Used in an Experimental Cloud Motion Wind Inferring System**
Z Wang, K A Browning and G A Kelly
October 1997

79. **A Preliminary Study of Fourier Series Analysis for Cloud Tracking with GOES High Temporal Resolution Images**
Z Wang
October 1997

80. **Analysis of an ex-tropical cyclone after reintensifying as a warm-core extratropical cyclone**
K A Browning, G Vaughan and P Panagi
November 1997

81. **A JCMM overview of FASTEX IOPs**
S A Clough, H W Lean, N M Roberts, H Birkett, J-P Chaboureau, R Dixon, M Griffiths, T D Hewson and A Montani
January 1998

82. **Programs for PV Inversion and Modification**
Meral Demirtas
December 1997

83. **Release of potential shearing instability in warm frontal zones**
D Chapman and K A Browning
February 1998

84. **The European Cloud-Resolving Modelling Programme (EUCREM)**
Summary Report from the coordinator
P W White
April 1998

85. **A Frontal Wave Database**
T D Hewson
April 1998

Met Office Joint Centre for Mesoscale Meteorology Department of Meteorology
University of Reading PO Box 243 Reading RG6 6BB United Kingdom
Tel: +44 (0)118 931 8425 Fax: +44 (0)118 931 8791
www.metoffice.com